



Pairing and non-Fermi liquid behavior in partially flat-band systems: Beyond nesting physicsSharareh Sayyad ^{1,2,*} Edwin W. Huang,^{3,4} Motoharu Kitatani,⁵ Mohammad-Sadegh Vaezi,^{6,7} Zohar Nussinov,⁷ Abolhassan Vaezi,^{3,8,9,†} and Hideo Aoki ^{10,11}¹*Institute for Solid State Physics, University of Tokyo, Kashiwanoha, Kashiwa, Chiba 277-8581, Japan*²*University Grenoble Alpes, CNRS, Grenoble INP, Institut Néel, 38000 Grenoble, France*³*Department of Physics, Stanford University, Stanford, California 94305, USA*⁴*Stanford Institute for Materials and Energy Sciences, SLAC National Accelerator Laboratory and Stanford University, Menlo Park, California 94025, USA*⁵*Institute of Solid State Physics, Vienna University of Technology, A-1040 Vienna, Austria*⁶*Pasargad Institute for Advanced Innovative Solutions (PIAIS), Tehran 1991633361, Iran*⁷*Department of Physics, Washington University, St. Louis, Missouri 63160, USA*⁸*Stanford Center for Topological Quantum Physics, Stanford University, Stanford, California 94305-4045, USA*⁹*Department of Physics, Sharif University of Technology, Tehran 14588-89694, Iran*¹⁰*National Institute of Advanced Industrial Science and Technology (AIST), Tsukuba 305-8568, Japan*¹¹*Department of Physics, University of Tokyo, Hongo, Tokyo 113-0033, Japan*

(Received 27 March 2019; published 6 January 2020)

While many-body effects in flat-band systems are receiving renewed hot interest in condensed-matter physics for superconducting and topological properties as well as for magnetism, studies have primarily been restricted to multiband systems (with coexisting flat and dispersive bands). Here we focus on *one-band* systems where a band is “partially flat,” comprising flat and dispersive portions in k space to reveal whether intriguing correlation effects can already arise on the simplest possible one-band level. For that, the two-dimensional repulsive Hubbard model is studied for two models having different flat areas in an intermediate-coupling regime with the dynamical mean-field theory combined with the fluctuation exchange approximation. We have a crossover from ferromagnetic to antiferromagnetic spin fluctuations as the band filling is varied and this triggers, for the model with a wider flat portion, a triplet-pair superconductivity favored over an unusually wide filling region, which is taken over by a sharply growing singlet pairing. For the model with a narrower flat portion, T_C against filling exhibits an unusual *double-peaked* T_C dome, associated with different numbers of nodes in the gap function having remarkably extended pairs in real space. We identify these as a manifestation of the physics outside the conventional nesting physics where only the pair scattering across the Fermi surface in designated (hot) spots is relevant. Another correlation effect arising from the flattened band is found in a non-Fermi-liquid behavior as detected in the momentum distribution function, frequency dependence of the self-energy, and spectral function. These indicate that unusual correlation physics can indeed occur in flat-band systems.

DOI: [10.1103/PhysRevB.101.014501](https://doi.org/10.1103/PhysRevB.101.014501)**I. INTRODUCTION**

While there is a long history for the study of flat-band systems as initiated by interest in ferromagnetism [1–5], there is a recent surge of interest in flat-band superconductivity, where possibilities are explored for unconventional superconductivity favored by the flat-band structure [6–9]. As for attractive electron-electron interactions, Törmä’s group has shown that a flat band can indeed favor superconductivity when the band is topological, with the superfluid weight lower-bounded by the topological number [10–14]. For repulsive interactions, on the other hand, a key question is how the presence of flat bands affects electron correlation processes. In repulsively interacting flat-band systems, spin alignment tends to lower the total energy due to unorthogonalizable Wannier orbitals through Pauli’s exclusion principle [3,8]. For unconventional

superconductivity, gap functions for both copper- and iron-based superconductors, respectively with d and $s\pm$ pairings, respectively, are maximized by the pair-scattering processes with specific momentum transfers (see Fig. 1, top left), where the spin fluctuations with these wave vectors glue electrons with opposite spins [15]. For systems having a flat band coexisting with dispersive band(s), it has been suggested that a key process is the quantum-mechanical virtual transfer of Cooper pairs between the flat and dispersive bands mediated by spin fluctuations arising from the repulsive interaction [6,8,16] (see Fig. 1, top right). There, it is noticed that an optimum situation is when the Fermi energy is close to, but away from, the flat band, where the virtual pair scattering still occurs. In other words, the flat band in this situation is “incipient” [17]. There, one intriguing observation is that the pairing, as detected from the density-matrix renormalization group, involves large entanglement when the flat band is topological [8].

These proposals for the flat-band magnetism and superconductivity have so far focused on multiband systems, as exem-

* sharareh.sayyad@neel.cnrs.fr

† vaezi@stanford.edu

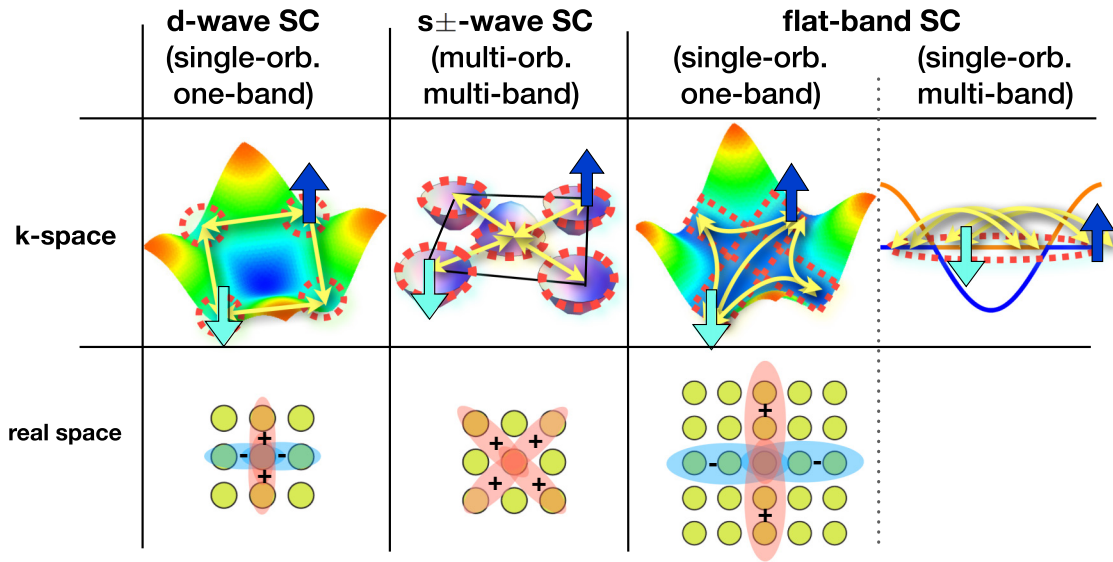


FIG. 1. We schematically compare an ordinary single-orbital, one-band case (here for a d -wave SC; leftmost column) and a multiorbital, multiband case (here for s_{\pm} ; second column from left), both with specific “hot spots” (dashed circles in red) across which the nesting vectors (yellow arrows) designate how pairs (blue and cyan arrows) scatter. These are contrasted with flat-band systems for the single-orbital, one-band case (second from right) and the single-orbital, multiband case (rightmost). The top row depicts k space, while the bottom row displays pairs in real space [18]. The pairing for the multiband case [6] is an interband s_{\pm} , which is difficult to represent in real space.

plified by Lieb’s, Mielke’s and Tasaki’s models, where one of the multibands is flat while other(s) are dispersive. Now, a fundamental question is, can interesting strong-correlation phenomena such as high T_C superconductivity occur in simpler *one-band* systems that have flat *portion(s)* in the dispersion in the momentum space? This is an interesting possibility, since, even when the Fermi energy resides on the dispersive part, quantum states are expected to be significantly altered through the virtual pair-scattering processes between the flat and dispersive portions of the band as well as the pair scatterings within the flat region, both with many channels (which turns out to be allowed due to partial occupation of the flat portion caused by correlation effects as we shall show; see Fig. 2). This will be outside the conventional “nesting physics” for dispersive bands where the processes occur on Fermi surfaces. Thus it is intriguing whether the one-band case can be as good as, or even better than, the multiband case. Motivated by these intuitions, here we explore two different flat-band models, where we start with a tight-binding (“ t - t' ”) model

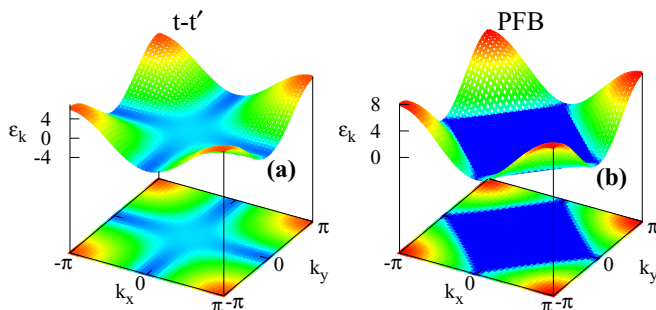


FIG. 2. One-electron band dispersions for the t - t' (a) and PFB (b) models. Blue region in (b) represents $\varepsilon_k = 0$.

with nearest- and second-neighbor hoppings. By controlling them, we have large flat regions in the dispersion with the vanishingly small group velocity. In the second model, we truncate the dispersion below a certain energy into a flat one to single out the effect of the flat part. Since the density of one-electron states diverges in these flat regions, perturbative approaches, e.g., the Schrieffer-Wolff transformation [19], might fail even in the weak electron-electron interaction regime. In Ref. [20], the truncated model is examined where the unbiased determinantal quantum Monte Carlo method (DQMC) [21,22] is used to show a Mott-insulating physics for a repulsive interaction and enhanced superconductivity for an attractive interaction in the weak-coupling regime and at intermediate temperatures, whereas the present paper addresses superconductivity for *repulsive* interactions. The flat portion also poses an interesting question of whether non-Fermi liquid behavior can arise due to the flatness.

Thus, the purpose of the present paper is to look into superconducting and non-Fermi liquid properties upon varying the band filling. For that, we adopt here, along with the DQMC method, the FLEX + DMFT method [23–25], which is a combination of the dynamical mean-field theory (DMFT) [26–28] and the fluctuation-exchange approximation (FLEX) [29,30]. The DQMC is a numerically exact method but is applicable for limited parameters. The FLEX + DMFT is a diagrammatic approximation and can deal with Mott’s insulation for strong coupling, but here we focus on an intermediate coupling regime. We shall show that magnetism exhibits a dominant ferromagnetic spin correlation at small band fillings, which crosses over to antiferromagnetic spin structures toward half filling. This concomitantly dominates superconductivity, where the pairing symmetry is found to change from spin triplet to singlet. Remarkably, the gap function sensitively depends on the Fermi energy sitting around the boundary

between the flat and dispersive parts in such a way that (i) for the truncated model with a wider flat portion, this triggers a triplet pairing favored over an unusually wide filling region, which is taken over by a sharply growing singlet pairing toward half filling. (ii) For the t - t' model with a narrower flat portion, T_C against filling exhibits an unusual *double-peaked* T_C dome associated with different numbers of nodes in the gap function. The unusually large numbers of nodal lines exhibit significantly extended pairs in real space in both models. Since these come from pair scatterings that involve the flat portions, we shall identify them as a manifestation of the physics outside the conventional nesting physics (with only the pair scattering across the Fermi surface in designated (hot) spots being relevant). We shall further reveal that a non-Fermi liquid behavior arises as detected in various observables such as a momentum distribution function that is fractional over the flat region, and the self-energy with a fractional-power-law frequency dependence accompanied by a characteristic spectral function. Thus we shall conclude that partially flat-band (PFB) systems can indeed harbor quite different and versatile physics from the ordinary bands.

II. MODEL AND METHODS

We consider the repulsive Hubbard model on the square lattice,

$$H = \sum_{k\sigma} \varepsilon_k c_{k\sigma}^\dagger c_{k\sigma} + U \sum_i n_{i\uparrow} n_{i\downarrow} - \mu \sum_{i\sigma} n_{i\sigma}, \quad (1)$$

where $c_{k\sigma}^\dagger$ creates an electron with spin σ and momentum \mathbf{k} , ε_k is the noninteracting band dispersion, $n_{i\sigma} = c_{i\sigma}^\dagger c_{i\sigma}$, $U (> 0)$ is the repulsive on-site interaction, and μ is the chemical potential.

Here we consider two models (Fig. 2): The first one is the t - t' model on a square lattice with the nearest-neighbor (t) and the second-neighbor (t') hoppings with a dispersion,

$$\varepsilon_k^{t-t'} = -2t[\cos(k_x) + \cos(k_y)] - 4t' \cos(k_x) \cos(k_y). \quad (2)$$

If we set $t' \simeq -t/2$, we can flatten the dispersion along Γ -M lines (with $t' = -0.548t$ here for minimizing the curvature) as displayed in Fig. 2(a).

The second model has a dispersion truncated as

$$\varepsilon_k^{\text{PFB}} = [1 + \mathcal{F} \operatorname{sgn}(\varepsilon_k^{\text{cosine}})] \varepsilon_k^{\text{cosine}}, \quad (3)$$

to have a perfectly flat bottom (hereafter PFB). Here $\varepsilon_k^{\text{cosine}} \equiv -2t[\cos(k_x) + \cos(k_y)]$ is the cosine band for the nearest-neighbor-hopping model, and the parameter \mathcal{F} controls the truncation, e.g., for $\mathcal{F} = 1$ the negative-energy part of the cosine band is flattened as displayed in Fig. 2(b). To have the same total band width ($=8$) as the cosine band, we set $\varepsilon_k^{\text{PFB}} = 2\varepsilon_k^{\text{cosine}}$ for the positive part when $\mathcal{F} = 1$. In this paper, we take t as the unit of energy.

As for the band filling, $\langle n \rangle = \langle n_\uparrow \rangle + \langle n_\downarrow \rangle$, the noninteracting Fermi energy lies close to the flat region for $\langle n \rangle \lesssim 1$. Here we study paramagnetic phases with no spin imbalance, basically with FLEX + DMFT. In FLEX + DMFT, the local self-energy is obtained from the DMFT procedure, with the FLEX local self-energy subtracted to avoid double counting

in a double self-consistent loop [23]. As an impurity solver for the DMFT, we adopt the modified iterative perturbation theory [31,32]. With FLEX + DMFT, we do not address here the strong-coupling regime for U exceeding the bandwidth, nor very dilute fillings for convergence reasons. For U greater than the bandwidth, employing the continuous-time quantum Monte Carlo [33] or the one-crossing approximation [34] as the impurity solver incorporates dynamical vertex corrections more properly but, independent of the impurity solver, our FLEX + DMFT formalism suffers from a lack of vertex corrections in spatial fluctuations. To sanity check and benchmark our FLEX + DMFT results, we compare them with DQMC results at relatively high temperatures where the sign problem is less severe. More precisely, in the DQMC, the fermionic sign problem makes the accessible temperature (T) for $U \leq 2$ restricted to $T \leq U/15$, see also Ref. [20], while we can go to lower T s in FLEX + DMFT. DQMC simulations are performed on a 16×16 periodic cluster, while FLEX + DMFT is performed for a 64×64 momentum grid.

III. RESULTS

Let us start with the double occupancy of electrons against the band filling in Fig. 3. We first recall that, for the ordinary cosine band, the double occupancy starts to increase in the strong-coupling regime and above half filling ($\langle n \rangle > 1$), where the number of electrons exceeds the number of lattice sites, see inset of Fig. 3 and also Ref. [20]. If we first look at the result for the PFB model, we can see quite a different behavior, where the double occupancy starts to grow already around $\simeq 0.6$ well below half filling, in both FLEX + DMFT [squares in Fig. 3(b)] and DQMC results (solid curves). We can particularly note that even at a very weak $U = 0.5$, the double occupancy arises when significantly less than half filled ($\langle n \rangle \gtrsim 0.6$), which can only occur in the cosine band above $\langle n \rangle \simeq 1$ at strong $U \gg$ bandwidth. Thus we deduce that the flat region makes the weak interaction sufficient for the emergence of the correlation effect. To endorse this, we turn to the double occupancy for the t - t' model obtained with FLEX + DMFT [solid curves in Fig. 3(a)]. We again encounter the double occupancy well below the half filling. The double occupancy in the t - t' model is greater than in the PFB, which is understandable since the flat region in the former is much narrower.

We can then examine the electron configuration in the momentum space to compare between the flat and dispersive parts (i.e., how electrons doubly occupy the flat regions before the dispersive regions are filled). Figure 4 presents the momentum-dependent distribution function $n_k = \frac{1}{2} \sum_{\sigma} \langle c_{k\sigma}^\dagger c_{k\sigma} \rangle$, where panel (a) is for the t - t' model at a filling $\langle n \rangle = 0.5$, while (b) is for the PFB at $\langle n \rangle = 0.62$, both for $U = 2$. The chosen fillings are, respectively, around the fillings at which the double occupancy starts to rise in Fig. 3. The figure is obtained with FLEX + DMFT, but we again observe a qualitative agreement between DQMC and FLEX + DMFT results (see Appendix A). For the t - t' model at $\langle n \rangle \simeq 0.5$, the occupation in the flat region along $k_x = 0$ and $k_y = 0$ is close to, but smaller than, unity with $0.7 < n_k < 0.85$. For the PFB model at $\langle n \rangle = 0.62$, we can see an almost constant and half-filled $0.52 < n_k < 0.55$ over the flat region

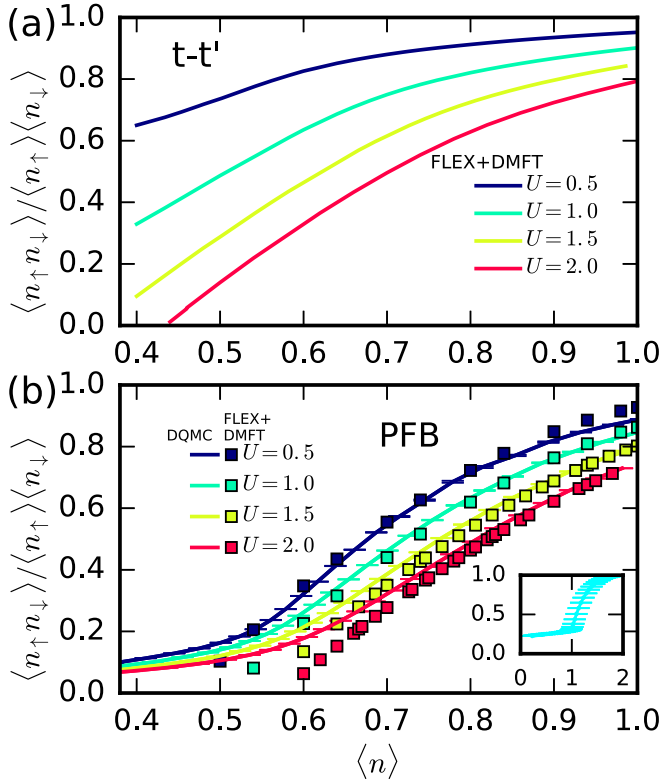


FIG. 3. Double occupancy [normalized by the uncorrelated value ($\langle n_{\uparrow} \rangle \langle n_{\downarrow} \rangle = \langle n \rangle^2 / 4$)] against the band filling $\langle n \rangle$ for the $t-t'$ [solid curves in (a)] and iPFB [squares in (b)] models, obtained with the FLEX + DMFT. Solid curves with error bars in (b) represent DQMC result for the PFB model [20]. The results are for $U = 0.5 - 2.0$ at temperature $T = U/15$. Inset in (b) is the double occupancy for the cosine band for $U = 12$ at the same temperature with DQMC. Error bars are determined by jackknife resampling.

bounded by $|k_x| + |k_y| \leq \pi$ in that model. Larger occupation in the $t-t'$ model should again be related to its narrower flat region.

The above results show that the electrons are selectively *crammed* into the flat portion, causing double occupation before the dispersive portion starts to be occupied. This would not be surprising since the flat portions are situated at lower

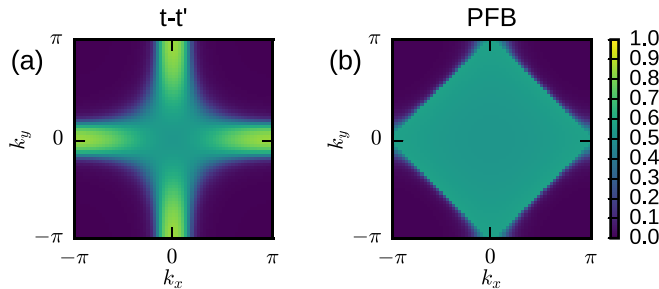


FIG. 4. (a) Momentum-dependent distribution function n_k for the $t-t'$ model at $\langle n \rangle = 0.5$. (b) The same for the PFB model at $\langle n \rangle = 0.62$. Results are computed with FLEX + DMFT on a 64×64 momentum grid. We have $U = 2$ and an inverse temperature $\beta = 7.5$ for both results.

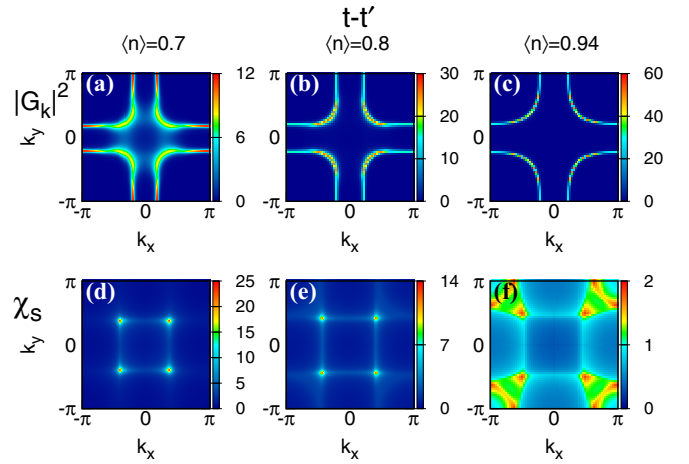


FIG. 5. For the $t-t'$ model, Green's functions (top panels) and spin susceptibilities (bottom) are color-coded in momentum space for fillings $\langle n \rangle = 0.7$ (a), (d); 0.8 (b), (e); and 0.94 (c), (f). All the results are for $U = 3$, $\beta = 33$, but note different color codes for different panels.

energies, but a remarkable point is the following: (i) The occupation is fractional, somewhere between the single and double occupations, and (ii) the occupation occurs all over the flat portions with basically the same occupied area as we vary the total band filling (compare Fig. 4 with Fig. 12 in Appendix B) in both models. In this sense, Luttinger's theorem [35] does not seem to apply here. To explore the Fermi surface formation, we plot the Green's function for both models in Figs. 5 and 6 (top panels), where sharp peaks would define the Fermi surfaces. While the Fermi surfaces are visible in the $t-t'$ model (Fig. 5), they are not very well-defined for the PFB model (Fig. 6). We come back to this point below in terms of the frequency dependence of the self-energy.

Let us now turn to the spin structure against the band filling. The static spin correlation function, $\chi_s(\mathbf{k}) = 2 \int_0^\beta d\tau \langle S_k^z(\tau) S_{-k}^z(0) \rangle$ [36] is displayed for the $t-t'$ (Fig. 5)

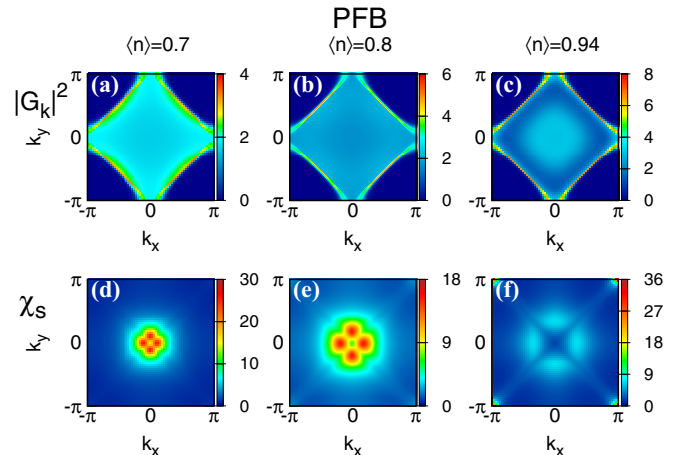


FIG. 6. The same as in the previous figure for the PFB model. In panel (f), maxima exist at $(\pm\pi, \pm\pi)$.

and PFB (Fig. 6) models at $U = 3$, $\beta \equiv 1/(k_B T) = 33$ and $\langle n \rangle = 0.7 - 0.94$. Overall, the spin correlation is seen to be large over *streaks* or wide *plateaus* (rather than usual spots), which should come from the flattened bands. More precisely, reflecting the structure of Green's function, the t - t' model shows streaks across some midpoints in the Brillouin zone, which cross over to wider and more complex structures as we approach $\langle n \rangle = 1$. A smaller overall value of the spin susceptibility in Fig. 5(f) may be attributed to coexistence of spin fluctuations coming from occupied flat and dispersive portions. The PFB model, on the other hand, shows a crossover from ferromagnetic spin fluctuations, which is expected as in the spin alignment in the half-filled flat branch in multiband models, to wider plateaus with peaks shifting away from Γ point, and finally to antiferromagnetic spin fluctuations with peaks around $(\pm\pi, \pm\pi)$ as we approach $\langle n \rangle = 1$. As for the charge susceptibility, $\chi_c(\mathbf{q}) = \int_0^\beta d\tau \langle n_{\mathbf{q}}(\tau) n_{-\mathbf{q}}(0) \rangle$, we observe a similar trend in both models, but χ_c is an order of magnitude smaller than the spin susceptibility. We shall see below that the spin structure governs the structures of the self-energy, local spectral function as well as pairing.

Now we are in position to explore the superconducting phases with the linearized Eliashberg equation for the gap function Δ ,

$$\lambda \Delta(k) = -\frac{1}{\beta} \sum_{k'} V_{\text{eff}}(k-k') G(k') G(-k') \Delta(k'), \quad (4)$$

where λ is the eigenvalue, $k \equiv (\mathbf{k}, i\omega_n)$ with ω_n being the Matsubara frequency with $\sum_{\mathbf{k}} = 1$, $V_{\text{eff}} = U + 3U^2\chi_s/2 - U^2\chi_c/2$ is the effective pairing interaction, and G is Green's function. The eigenvalue is a measure of superconducting instabilities with $\lambda = 1$ marking T_C . Figure 7, a key result of this work, plots λ for singlet (filled symbols) and triplet (empty) pairings for the t - t' and PFB models.

If we first look at the result for the PFB model, triplet pairing is favored with larger λ s over a remarkably wide region of the filling, which indicates the importance of the wide flat region accompanied by ferromagnetic fluctuations. Then a singlet pairing rapidly dominates as we approach $\langle n \rangle = 1$. In the t - t' model, with a narrower flat portion and associated spin fluctuations (Fig. 5), singlet pairing dominates over the whole region studied here, but with a curious *double-dome* structure in T_C . Both of these are in dramatic contrast with the usual cosinelike bands, where the singlet d -wave pairing dominates with a single dome in λ around $\langle n \rangle \approx 0.9$ [23,25,37]. The sharp enhancement in the singlet pairing close to the half-filling in the PFB, which should come from the prevailing antiferromagnetic fluctuations, has λ that is larger than t - t' and even the cosine-band counterparts. We note that this takeover [an arrow in Fig. 7(b)] occurs when the flat-band filling exceeds about 3/4 (see Appendix B), which in fact coincides with a critical filling, $\langle n \rangle_c$, at which the DMFT spin susceptibility is peaked (see Appendix C) and the exponent in the self-energy is also peaked as we shall see in Fig. 10(b) below. As for the singlet pairing in the t - t' model, we can see that the left peak in λ occurs around $\langle n \rangle_c$ for this model.

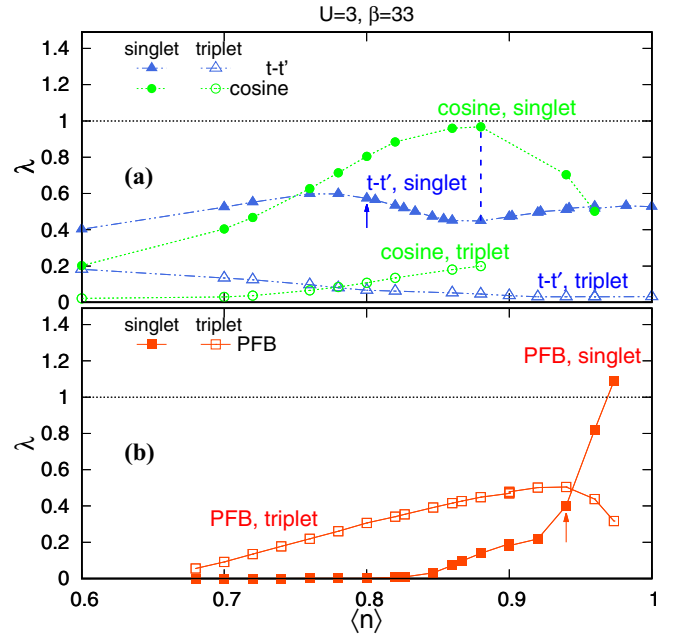


FIG. 7. Largest eigenvalue λ of the Eliashberg equation versus the filling for the singlet (filled symbols) and triplet (empty) pairings for t - t' (triangles) (a), cosine-band (circles) (a), and PFB (squares) (b) models for $U = 3$, $\beta = 33$. Arrows indicate the $\langle n \rangle_c$ at which the spin susceptibility is peaked for respective models, while the dashed vertical line indicates a change in the pairing symmetry, see text.

So let us now fathom these results in terms of filling-dependent singlet and triplet gap functions in momentum space in Fig. 8, or in real space in Fig. 9, for the t - t' and PFB models. We can immediately see that all the gap functions are anisotropic and possess nodal lines whose number sensitively depends on the filling. In the t - t' model, cases similar to the usual d -wave [$\Delta(\mathbf{k}) \sim \cos(k_x) - \cos(k_y)$] exist [as in Figs. 8(b) and 9(b)], but more generally admits structures, $\Delta_{\text{singlet}}(\mathbf{k}) \sim \cos(\gamma k_x) - \cos(\gamma k_y)$, where $\gamma (= 1, 2, \dots)$ characterizes the number of nodal lines. For instance, we have $\gamma = 1 \rightarrow 2$ for $\langle n \rangle = 0.94 \rightarrow 0.7$ in the t - t' model. This shows that, as we go away from the half filling at which antiferromagnetic fluctuations dominate, the usual $d_{x^2-y^2}$ wave changes into something more complicated.

If we turn to the gap functions in real space in Fig. 9, we can realize that the larger the number of nodal lines, the more extended the pairs over several lattice spacings in real space. Similar long-range pairings have also been explored for quasi-one-dimensional and 2D systems [38,39], where each pair becomes more spatially extended as we go from p -wave to d and f with the number of nodes increasing. For the triplet gap function [40] in Figs. 8(c), 8(d), 8(g), and 8(h), we also tend to have unusually extended pairing with larger numbers of nodes. In the literature, the random-phase approximation (RPA) has been used to obtain the filling-dependent gap symmetry in the t - t' model [41], but the present results exhibit different behavior such as an absence of s -waves seen in RPA, which should be due to the self-energy effects incorporated more accurately here. For the PFB model, triplet gap functions

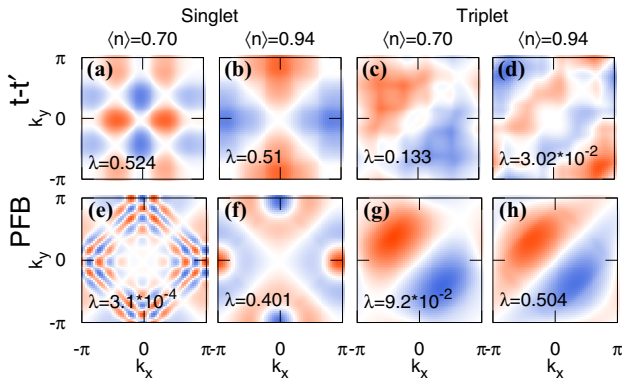


FIG. 8. Singlet (left four panels) and triplet (right four panels) gap functions in momentum space for the t - t' (first row) and PFB (second row) models. Filling is $\langle n \rangle = 0.7$ (a), (c), (e), (g) or 0.94 (b), (d), (f), (h). For each of the triplet cases, another one rotated by 90 degrees is degenerate due to the tetragonal symmetry of the lattice. Maximum eigenvalue of the Eliashberg equation is indicated in each panel. Color code for the gap function is bluish (reddish) for negative (positive) values, for which we have omitted the color bars since the linearized Eliashberg equation does not indicate magnitudes of Δ . All the results are for $U = 3$, $\beta = 33$. Note that the λ in (d), (e), (g) is vanishingly small ($<10^{-1}$), so should not be taken seriously.

are close to a simple p -wave, $\Delta_{\text{triplet}}(\mathbf{k}) \sim \sin(k_x) \pm \sin(k_y)$, but extra nodes are visible.

If we go back to Fig. 7, the Eliashberg λ in our partially-flat band systems can be smaller than those for the ordinary cosine band, which may be related to less compact pairing in the former, but we do have important effects peculiar to the flat-band cases: For the PFB, (i) the singlet λ sharply blows up toward the filling $n = 1$ and (ii), before this occurs, the triplet pairings are favored over an unusually wide region of n . For t - t' , (iii) the peculiar double-peak structure arises from a change in the number of nodes around the dip of λ [marked with a vertical dashed line in Fig. 7(a)]. If we compare the single-band and multiband flat-band systems [42], the former sharply contrasts with the behavior of the multiband case [16] in which the Eliashberg λ is shown to have a sharp dip when

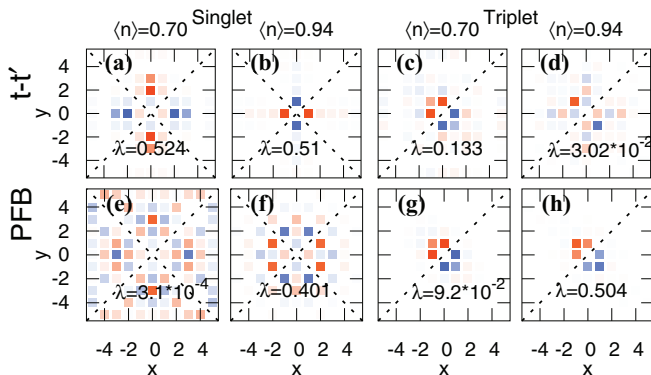


FIG. 9. The same as in the previous figure in real space. Dashed lines represent nodes.

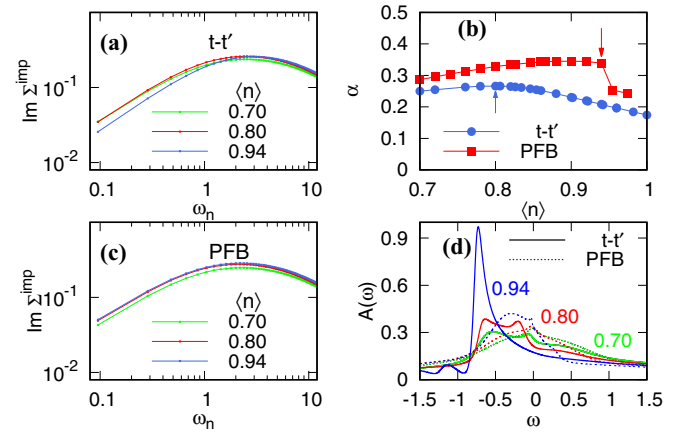


FIG. 10. Imaginary part of the DMFT impurity self-energy, Σ_{imp} , against Matsubara frequency, ω_n , for $\langle n \rangle = 0.7$ (green), 0.9 (red), 0.94 (blue) in the t - t' (a) and PFB (c) models. (b) The exponent α in the fit $|\text{Im}\Sigma_{\text{imp}}(i\omega_n)| \propto \omega_n^\alpha$, for the t - t' (blue circles) and PFB (red squares) models. Arrows mark respective $\langle n \rangle_c$ for the spin susceptibility peaks, which are seen here to coincide with the peaks in α . (d) Local spectral functions in the t - t' (solid lines) and PFB (dotted) models for the band filling $\langle n \rangle = 0.7, 0.8, 0.94$. All the results are for $U = 3$ and $\beta = 33$.

E_F becomes too close to the flat band, but this does not occur in the present single-band case.

Fermi-liquid properties

We finally look into the Fermi-liquid properties. In Figs. 10(a) and 10(c), we plot the imaginary part of the DMFT self-energies against Matsubara frequency in the t - t' (a) and PFB (c) models, for band filling $\langle n \rangle = 0.7 - 1.0$ at $U = 3$, $\beta = 33$. We notice that the self-energy exhibits a peculiar frequency dependence. We can actually quantify non-Fermi liquid behavior by fitting the imaginary part of the self-energy to

$$|\text{Im}\Sigma_{\text{imp}}(i\omega_n)| \propto \omega_n^\alpha,$$

for low Matsubara frequencies. Then $\alpha = 1$ characterizes the Fermi liquids, while $\alpha < 0.5$ will signify a “bad-metallic” behavior [43–45]. Here we take the DMFT impurity self-energy, Σ_{imp} , since we want to look at the local self-energy, which we shall later compare with the DMFT impurity spin-susceptibility. We can see in Fig. 10(b) that the exponent α increases up to a critical filling $\langle n \rangle_c$ that depends whether we have the t - t' or PFB models. It is notable that the $\langle n \rangle_c$ for the self-energy coincide with the critical $\langle n \rangle_c$ ($= 0.82$ for t - t' , $\langle n \rangle_c = 0.94$ for PFB at $U = 3$, $\beta = 33$) at which the spin susceptibility for the DMFT impurity, χ_s^{imp} , has a peak in each model, as shown in Appendix C. For further increase of the filling, α starts to decrease. The value $\langle n \rangle_c = 0.94$ in the PFB corresponds to the filling at which the flat part of the band is about $3/4$ filled, namely, we have $0.71 < n_k < 0.83$ on the flat portion in the momentum-dependent distribution function (see Appendix B). A bad-metallic behavior also appears as deformations in the local spectral functions in Fig. 10(d), obtained via analytic continuation with the Padé approximation. In particular, the local spectral functions undergo large

changes for $\langle n \rangle > \langle n \rangle_c$ with an emergence of multipeaks that are separated by $\omega \ll U$, see also Appendix D.

IV. CONCLUSION AND DISCUSSIONS

To summarize, we have studied two partially-flat band models (t - t' and PFB) to reveal that a manifestation of the flat portion in the band gives a dramatic difference from the ordinary band to produce a peculiar sequence of the dominant pairing symmetries. This occurs in both models, in a manner that is dominated by the size of the flat region. For PFB with a wide flat area, triplet pairings are favored over a wide filling region, while for t - t' with a narrower flat area, a double-dome structure in T_C emerges associated with different numbers of nodes in the gap function. Concomitantly, pairings can become unusually extended in real space with large numbers of nodes. We have finally shown that non-Fermi-liquid like behavior exists in a power-law frequency dependence of the self-energy, etc. We identify these as a peculiar emergence of correlation effects in partially-flat band systems that can occur even for intermediate electron-electron interactions.

As Fig. 1 suggests, the different pairings revealed here should come from quite different configurations of pair-scattering channels in the partially-flat band models: In regular bands, the key process is the pair scattering specifically between the “hot spots” (antinodal regions in the cuprates, and Fermi pockets in the iron-based superconductors [15], respectively, giving rise to the d and s_{\pm} pairings), which is contrasted with the flat bands that have the whole *bunch* of pair-scattering channels involving, so to speak, “extended hot regions.”

This now leads us to make an observation: For ordinary bands, we can show, from a general phase-space volume argument [46,47], that the superconductivity mediated by spin fluctuations should work much more efficiently in two-dimensional (layered 2D) systems than in 3D. By contrast, the flat bands with (i) extended hot regions (with wide areas in k space for large spin fluctuations), (ii) wide areas for large gap function amplitudes, and (iii) also wide areas for large Green’s functions [which are involved in Eq. (4)] may *evade* the above theorem to render 3D systems as good as in 2D. This will make 3D partially-flat band systems interesting.

An important question, of course, is whether flat bands can enhance T_C . For the attractive Hubbard model, the sign-free DQMC actually indicates that T_C is nearly doubled when the band is flattened into PFB [20]. A general question then is whether T_C is enhanced in the repulsive model, which is an important future problem. For ordinary (cosine) bands, Kitatani *et al.* have used D Γ A (dynamical vertex approximation) to identify the vertex correction as the reason why T_C ($\sim 0.01t$) in the spin-fluctuation mediated pairing is two orders of magnitude smaller than the starting electronic energy [37]. It will be interesting to see whether the vertex correction in the flat-band systems can act to overcome this. In the present flat-band models, the spin susceptibility can have broad structures such as plateaus. One possible hint is that Yanase *et al.* [48] show that the vertex correction becomes significant in a model that has a featureless spin structure.

As for vanishing group velocity, this also occurs point-like at van Hove singularities, and its effect on correlation physics has been discussed [49], where topological superconductivity such as $d + id$ wave is suggested. So it is intriguing to examine whether the present systems, where the group velocity vanishes in finite *areas* rather than at points, can accommodate topological superconductivity. The present paper has shown transitions between different pairing symmetries (within singlets with different numbers of nodes in t - t' and singlet-triplet transition in PFB). In fact, it is known that the boundary between different pairing symmetries is a promising venue for looking for time-reversal-broken topological superconductivity [50–52].

As for possible realizations of the present model, we can raise an example which is the τ -type organic salt family, $D_2A_1A_y$, based on D (=P-S, S-DMEDT-TTF or EDO-S, S-DMEDT-TTF) in combination with anions A (= AuBr₂, I₃, or IBr₂), studied by Papavassiliou *et al.* [53,54], which are two-dimensional metals in the τ crystal form. The band structure of a single layer of the τ phase contains a flat-bottomed band just as in the present t - t' model. Indeed, a checkerboard-patterned organic molecule in the layer makes its effective model a tight-binding system with $t' \simeq -0.5t$ [53–56]. As for inorganic materials, ruthenate superconductors [57,58], and some iron-chalcogenides [59,60] have partially-flat bands. They are multiband systems, where competition between various pairing symmetries [61,62], fractional power-law behavior in the optical conductivity [63–65], and (anti)ferromagnetic spin structures [66,67] have been discussed. On the other hand, there is a recent upheaval of interest in twisted bilayer graphene, where the band structures are shown to have flat portions on hexagonal lattices [68–79]. This further highlights the need to understand partially-flat bands more generically. As for the space group, we can extend the present idea on tetragonal lattices to hexagonal cases, which is underway.

ACKNOWLEDGMENTS

Numerical calculations were performed on the REIMS cluster and the ISSP Supercomputer in the University of Tokyo, and on the Sherlock cluster at Stanford University. S.S. and H.A. acknowledge a support from the ImPACT Program of the Council for Science, Technology and Innovation, Cabinet Office, Government of Japan (Grant No. 2015-PM12-05-01) from JST. S.S. acknowledges funding from ANR-18-CE30-0001-01. H.A. thanks Kazuhiko Kuroki for illuminating discussions, and is also supported by JSPS KAKENHI Grants No. JP26247057, No. 17H06138, and CREST “Topology” project from JST. E.W.H. was supported by the U.S. Department of Energy (DOE), Office of Basic Energy Sciences, Division of Materials Sciences and Engineering, under Contract No. DE-AC02-76SF00515. M.S.V. and Z.N. acknowledge partial support by the National Science Foundation (NSF No. 1411229). M.S.V. also acknowledges the financial support from Pasargad Institute for Advanced Innovative Solutions (PIAIS) under Supporting Grant scheme (Project No. SG1-RCM1903-01).

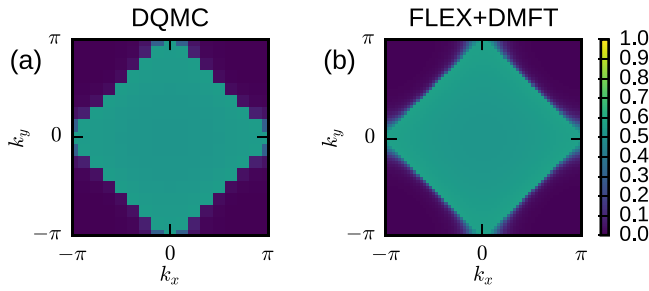


FIG. 11. Momentum distribution function for the PFB model computed with DQMC on a periodic 16×16 cluster (a), as compared with the result in FLEX + DMFT on a 64×64 momentum grid (b), for $U = 2$, inverse temperature $\beta = 7.5$, and filling $\langle n \rangle = 0.62$.

APPENDIX A: COMPARISON OF DQMC AND FLEX + DMFT RESULTS FOR MOMENTUM-DEPENDENT DISTRIBUTION FUNCTIONS

Let us here compare the momentum-dependent distribution functions obtained with the DQMC and FLEX + DMFT approaches for the PFB model at $\langle n \rangle = 0.62$ for $U = 2$, $\beta = 7.5$ in Fig. 11. The occupancy and shape of the occupied regions are seen to accurately agree between the two results. More precisely, the electron occupancy in the flat portions ranges from 0.52–0.55 in the DQMC (a) and 0.52–0.57 in the FLEX + DMFT (b).

APPENDIX B: MOMENTUM-DEPENDENT DISTRIBUTION FUNCTIONS AT $\langle n \rangle_c$ FOR THE $t-t'$ AND PFB MODELS

We display in Fig. 12 how the momentum-dependent distribution function, n_k , behaves right at the critical filling $\langle n \rangle_c = 0.82$ for $t-t'$, and 0.94 for the PFB model. The occupation of the flat portion of the band in the PFB system ranges from 0.71 to 0.83, i.e., about 3/4. In the $t-t'$ model, the flat portion is close to fully occupied, associated with the narrower size of the flat region of this band. These results should be compared with Fig. 4 in the main text, where the flat portion has an occupation about 1/2 in PFB.

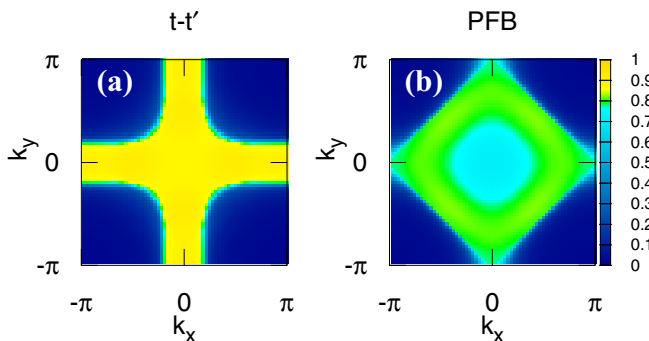


FIG. 12. Momentum-dependent distribution function, n_k , at the critical fillings, $\langle n \rangle_c = 0.82$ for the $t-t'$ (a) and 0.94 for the PFB (b) models, for $U = 3$ and $\beta = 33$.

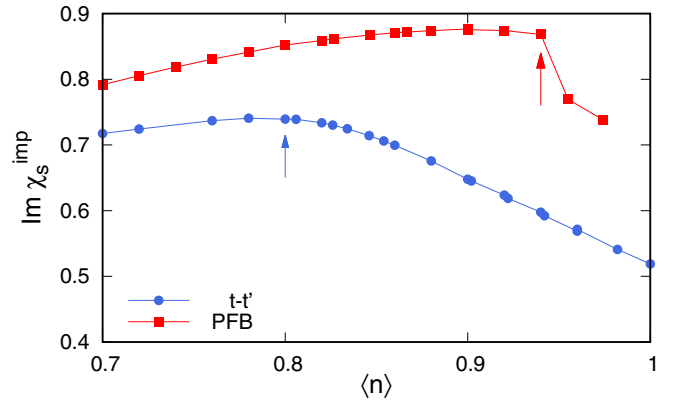


FIG. 13. DMFT impurity spin susceptibility against band filling for the $t-t'$ (blue circles) and PFB (red squares) models for $U = 3$ and $\beta = 33$. Arrows indicate the critical filling $\langle n \rangle_c$ in the two models, respectively.

APPENDIX C: DMFT IMPURITY SPIN-SUSCEPTIBILITY

Let us display in Fig. 13 the DMFT spin-susceptibility χ_s^{imp} , obtained from the DMFT impurity Green's functions, for $U = 3$ and inverse temperature $\beta = 33$ in the $t-t'$ and PFB models. The result exhibits a peak (marked, respectively, with an arrow) in each model, which is seen to coincide with the critical filling $\langle n \rangle_c$ for the self-energy behavior introduced in the main text, see the arrows in Figs. 7 and 10(b).

APPENDIX D: MOMENTUM-DEPENDENT SPECTRAL FUNCTIONS AT $\langle n \rangle_c$

We present the momentum-dependent spectral functions at $\Gamma(0, 0)$ and X $(0, \pi)$ points in the Brillouin zone right at the critical band filling, $\langle n \rangle = 0.81$ in $t-t'$ and $\langle n \rangle = 0.94$ in PFB models, in Fig. 14. The spectrum is obtained with Padé approximation. In both panels, shoulderlike features are seen at Γ point as a correlation effect. Such a feature also appears at $(0, \pi)$ in the PFB model. The result should be compared with the local spectral functions in Fig. 10(d) in the main text.

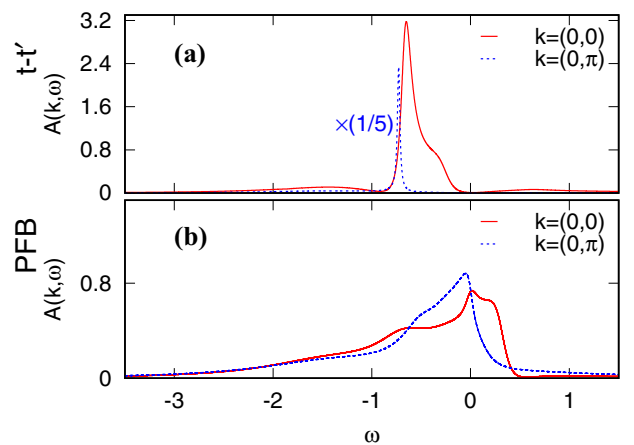


FIG. 14. Spectral function, $A(\mathbf{k}, \omega)$, at Γ (red solid lines) and X (blue dotted) points in $t-t'$ (a) and PFB (b) models for $U = 3$, $\beta = 33$, and band filling $\langle n \rangle = 0.81$ (a) or $\langle n \rangle = 0.94$ (b). Spectral function at X point in (a) is divided by a factor of 5.

- [1] E. H. Lieb, *Phys. Rev. Lett.* **62**, 1201 (1989).
- [2] A. Mielke, *J. Phys. A: Math. Gen.* **24**, 3311 (1991).
- [3] H. Tasaki, *Phys. Rev. Lett.* **69**, 1608 (1992).
- [4] A. Tanaka and H. Ueda, *Phys. Rev. Lett.* **90**, 067204 (2003).
- [5] H. Katsura, I. Maruyama, A. Tanaka, and H. Tasaki, *Europhys. Lett.* **91**, 57007 (2010).
- [6] K. Kuroki, T. Higashida, and R. Arita, *Phys. Rev. B* **72**, 212509 (2005).
- [7] M. Tovmasyan, E. P. L. van Nieuwenburg, and S. D. Huber, *Phys. Rev. B* **88**, 220510(R) (2013).
- [8] K. Kobayashi, M. Okumura, S. Yamada, M. Machida, and H. Aoki, *Phys. Rev. B* **94**, 214501 (2016).
- [9] V. J. Kauppila, F. Aikebaier, and T. T. Heikkilä, *Phys. Rev. B* **93**, 214505 (2016).
- [10] M. Tovmasyan, S. Peotta, P. Törmä, and S. D. Huber, *Phys. Rev. B* **94**, 245149 (2016).
- [11] R. Ojajarvi, T. Hyart, M. A. Silaev, and T. T. Heikkilä, *Phys. Rev. B* **98**, 054515 (2018).
- [12] M. Tovmasyan, S. Peotta, L. Liang, P. Törmä, and S. D. Huber, *Phys. Rev. B* **98**, 134513 (2018).
- [13] L. Liang, S. Peotta, A. Harju, and P. Törmä, *Phys. Rev. B* **96**, 064511 (2017).
- [14] L. Liang, T. I. Vanhala, S. Peotta, T. Siro, A. Harju, and P. Törmä, *Phys. Rev. B* **95**, 024515 (2017).
- [15] H. Hosono and K. Kuroki, *Phys. C* **514**, 399 (2015).
- [16] K. Matsumoto, D. Ogura, and K. Kuroki, *Phys. Rev. B* **97**, 014516 (2018).
- [17] The incipient band is the terminology used in the iron-based superconductors as in Qian *et al.*, *Phys. Rev. Lett.* **106**, 187001 (2011), but the concept is originally introduced by Ref. [6].
- [18] For the rightmost panels, we display the case of a quasi-one-dimensional cross-linked two-leg ladder considered in Ref. [6].
- [19] J. R. Schrieffer and P. A. Wolff, *Phys. Rev.* **149**, 491 (1966).
- [20] E. W. Huang, M.-S. Vaezi, Z. Nussinov, and A. Vaezi, *Phys. Rev. B* **99**, 235128 (2019).
- [21] S. R. White, D. J. Scalapino, R. L. Sugar, N. E. Bickers, and R. T. Scalettar, *Phys. Rev. B* **39**, 839 (1989).
- [22] S. R. White, D. J. Scalapino, R. L. Sugar, E. Y. Loh, J. E. Gubernatis, and R. T. Scalettar, *Phys. Rev. B* **40**, 506 (1989).
- [23] M. Kitatani, N. Tsuji, and H. Aoki, *Phys. Rev. B* **92**, 085104 (2015).
- [24] J. Gukelberger, L. Huang, and P. Werner, *Phys. Rev. B* **91**, 235114 (2015).
- [25] M. Kitatani, N. Tsuji, and H. Aoki, *Phys. Rev. B* **95**, 075109 (2017).
- [26] W. Metzner and D. Vollhardt, *Phys. Rev. Lett.* **62**, 324 (1989).
- [27] A. Georges and W. Krauth, *Phys. Rev. Lett.* **69**, 1240 (1992).
- [28] A. Georges, G. Kotliar, W. Krauth, and M. J. Rozenberg, *Rev. Mod. Phys.* **68**, 13 (1996).
- [29] N. Bickers and D. Scalapino, *Ann. Phys.* **193**, 206 (1989).
- [30] N. E. Bickers, D. J. Scalapino, and S. R. White, *Phys. Rev. Lett.* **62**, 961 (1989).
- [31] L.-F. Arsenault, P. Sémon, and A.-M. S. Tremblay, *Phys. Rev. B* **86**, 085133 (2012).
- [32] H. Kajueter and G. Kotliar, *Phys. Rev. Lett.* **77**, 131 (1996).
- [33] E. Gull, A. J. Millis, A. I. Lichtenstein, A. N. Rubtsov, M. Troyer, and P. Werner, *Rev. Mod. Phys.* **83**, 349 (2011).
- [34] V. Vildosola, L. V. Pourovskii, L. O. Manuel, and P. Roura-Bas, *J. Phys.: Condens. Matter* **27**, 485602 (2015).
- [35] See, e.g., K. Limtragool, Z. Leong, and P. W. Phillips, *SciPost Phys.* **5**, 049 (2018).
- [36] W. A. Roshen and J. Ruvalds, *Phys. Rev. B* **28**, 1329 (1983).
- [37] M. Kitatani, T. Schäfer, H. Aoki, and K. Held, *Phys. Rev. B* **99**, 041115(R) (2019).
- [38] Y. Tanuma, K. Kuroki, Y. Tanaka, R. Arita, S. Kashiwaya, and H. Aoki, *Phys. Rev. B* **66**, 094507 (2002).
- [39] K. Kuroki, Y. Tanaka, T. Kimura, and R. Arita, *Phys. Rev. B* **69**, 214511 (2004).
- [40] A possibility of triplet pairing in the t - t' model has been studied in, e.g., R. Arita, K. Kuroki, and H. Aoki, *J. Phys. Soc. Jpn.* **73**, 533 (2004); A. Kauch, F. Hörbinger, G. Li, and K. Held, *arXiv:1901.09743*.
- [41] A. T. Rømer, A. Kreisel, I. Eremin, M. A. Malakhov, T. A. Maier, P. J. Hirschfeld, and B. M. Andersen, *Phys. Rev. B* **92**, 104505 (2015).
- [42] We can note in passing that T. Misumi and H. Aoki, *Phys. Rev. B* **96**, 155137 (2017), propose a class of models where a flat band pierces right in the middle of a dispersive band, so each band in this system is a partially flat band.
- [43] P. Werner, E. Gull, M. Troyer, and A. J. Millis, *Phys. Rev. Lett.* **101**, 166405 (2008).
- [44] H. Ishida and A. Liebsch, *Phys. Rev. B* **81**, 054513 (2010).
- [45] P. Werner, S. Hoshino, and H. Shinaoka, *Phys. Rev. B* **94**, 245134 (2016).
- [46] R. Arita, K. Kuroki, and H. Aoki, *Phys. Rev. B* **60**, 14585 (1999).
- [47] P. Monthoux and G. G. Lonzarich, *Phys. Rev. B* **59**, 14598 (1999).
- [48] Y. Yanase, T. Jujo, T. Nomura, H. Ikeda, T. Hotta, and K. Yamada, *Phys. Rep.* **387**, 1 (2003).
- [49] C.-C. Liu, L.-D. Zhang, W.-Q. Chen, and F. Yang, *Phys. Rev. Lett.* **121**, 217001 (2018).
- [50] R. M. Fernandes and A. J. Millis, *Phys. Rev. Lett.* **111**, 127001 (2013).
- [51] F. Ahn, I. Eremin, J. Knolle, V. B. Zabolotnyy, S. V. Borisenko, B. Büchner, and A. V. Chubukov, *Phys. Rev. B* **89**, 144513 (2014).
- [52] R. Oiwa, Y. Yanagi, and H. Kusunose, *J. Phys. Soc. Jpn.* **88**, 063703 (2019).
- [53] G. Papavassiliou, D. Lagouvardos, A. Terzis, C. Raptopoulou, B. Hilti, W. Hofherr, J. Zambounis, G. Rihs, J. Pfeiffer, P. Delhaes, K. Murata, N. Fortune, and N. Shirakawa, *Synth. Met.* **70**, 787 (1995), Proceedings of the International Conference on Science and Technology of Synthetic Metals.
- [54] H. Aizawa, K. Kuroki, H. Yoshino, G. A. Mousdis, G. C. Papavassiliou, and K. Murata, *J. Phys. Soc. Jpn.* **83**, 104705 (2014).
- [55] R. Arita, K. Kuroki, and H. Aoki, *Phys. Rev. B* **61**, 3207 (2000).
- [56] As discussed in Ref. [55], in the tight-binding model for the τ conductor, the in-plane molecular configuration is such that the second-neighbor intermolecular hopping, $t_2 \simeq 0.02$ eV, appears in every other plaquette in a checkerboard manner on top of the nearest $t_1 \simeq 0.2$ eV. The checkerboard makes the Brillouin zone folded, where the dispersion of the upper band in which E_F resides is expressed as (the square root of) the t - t' tight-binding dispersion with $t' = -0.5t$ when the splitting due to t_2 is small.
- [57] Q. H. Wang, C. Platt, Y. Yang, C. Honerkamp, F. C. Zhang, W. Hanke, T. M. Rice, and R. Thomale, *Europhys. Lett.* **104**, 17013 (2013).

- [58] C. Autieri, M. Cuoco, and C. Noce, *Phys. Rev. B* **89**, 075102 (2014).
- [59] P. D. Johnson, H.-B. Yang, J. D. Rameau, G. D. Gu, Z.-H. Pan, T. Valla, M. Weinert, and A. V. Fedorov, *Phys. Rev. Lett.* **114**, 167001 (2015).
- [60] A. Subedi, L. Zhang, D. J. Singh, and M. H. Du, *Phys. Rev. B* **78**, 134514 (2008).
- [61] K. Kuroki, M. Ogata, R. Arita, and H. Aoki, *Phys. Rev. B* **63**, 060506(R) (2001).
- [62] A. P. Mackenzie and Y. Maeno, *Rev. Mod. Phys.* **75**, 657 (2003).
- [63] Z. P. Yin, K. Haule, and G. Kotliar, *Phys. Rev. B* **86**, 195141 (2012).
- [64] C. Mirri, P. Calvani, F. M. Vitucci, A. Perucchi, K. W. Yeh, M. K. Wu, and S. Lupi, *Supercond. Sci. Technol.* **25**, 045002 (2012).
- [65] Y. S. Lee, J. S. Lee, T. W. Noh, D. Y. Byun, K. S. Yoo, K. Yamaura, and E. Takayama-Muromachi, *Phys. Rev. B* **67**, 113101 (2003).
- [66] H. Kawanaka, Y. Aiura, T. Hasebe, M. Yokoyama, T. Masui, Y. Nishihara, and T. Yanagisawa, *Sci. Rep.* **6**, 35150 (2016).
- [67] H. Kotegawa and M. Fujita, *Sci. Technol. Adv. Mater.* **13**, 054302 (2012).
- [68] Y. Cao, V. Fatemi, S. Fang, K. Watanabe, T. Taniguchi, E. Kaxiras, and P. Jarillo-Herrero, *Nature* **556**, 43 (2018).
- [69] Y. Cao, V. Fatemi, A. Demir, S. Fang, S. L. Tomarken, J. Y. Luo, J. D. Sanchez-Yamagishi, K. Watanabe, E. Kaxiras, R. C. Ashoori, and P. Jarillo-Herrero, *Nature* **556**, 80 (2018).
- [70] M. Koshino, N. F. Q. Yuan, T. Koretsune, M. Ochi, K. Kuroki, and L. Fu, *Phys. Rev. X* **8**, 031087 (2018).
- [71] E. Suárez Morell, J. D. Correa, P. Vargas, M. Pacheco, and Z. Barticevic, *Phys. Rev. B* **82**, 121407(R) (2010).
- [72] R. Bistritzer and A. H. MacDonald, *Proc. Natl. Acad. Sci.* **108**, 12233 (2011).
- [73] E. J. Mele, *Phys. Rev. B* **81**, 161405(R) (2010).
- [74] G. Trambly de Laissardière, D. Mayou, and L. Magaud, *Nano Lett.* **10**, 804 (2010).
- [75] S. Fang and E. Kaxiras, *Phys. Rev. B* **93**, 235153 (2016).
- [76] G. Chen, A. L. Sharpe, P. Gallagher, I. T. Rosen, E. J. Fox, L. Jiang, B. Lyu, H. Li, K. Watanabe, T. Taniguchi, J. Jung, Z. Shi, D. Goldhaber-Gordon, Y. Zhang, and F. Wang, *Nature* **572**, 215 (2019).
- [77] S. Moriyama, Y. Morita, K. Komatsu, K. Endo, T. Iwasaki, S. Nakaharai, Y. Noguchi, Y. Wakayama, E. Watanabe, D. Tsuya, K. Watanabe, and T. Taniguchi, [arXiv:1901.09356](https://arxiv.org/abs/1901.09356).
- [78] E. Codecido, Q. Wang, R. Koester, S. Che, H. Tian, R. Lv, S. Tran, K. Watanabe, T. Taniguchi, F. Zhang, M. Bockrath, and C. N. Lau, [arXiv:1902.05151](https://arxiv.org/abs/1902.05151).
- [79] H. C. Po, L. Zou, T. Senthil, and A. Vishwanath, *Phys. Rev. B* **99**, 195455 (2019).